Exclusive D_{s} semileptonic branching fraction measurements

J. Hietala, D. Cronin-Hennessy, T. Pedlar, and I. Shipsey

Phys. Rev. D **92**, 012009 — Published 17 July 2015

DOI: 10.1103/PhysRevD.92.012009

Exclusive D_s semileptonic branching fraction measurements

J. Hietala,[1,*] D. Cronin-Hennessy,[1,†] T. Pedlar,[2] and I. Shipsey[3]

[1] *Department of Physics, University of Minnesota, Minneapolis, Minnesota 55455, USA*
[2] *Department of Physics, Luther College, Decorah, Iowa 52101, USA*
[3] *Sub-department of Particle Physics, Oxford OX1 3RH, United Kingdom*

We measure absolute branching fractions for six exclusive D_s semileptonic decays. We use data collected in the CLEO-c detector from e^+e^- annihilations delivered by the Cornell Electron Storage Ring with a center-of-mass energy near 4170 MeV. We find $\mathcal{B}(D_s \to \phi e\nu) = (2.14 \pm 0.17 \pm 0.08)\%$, $\mathcal{B}(D_s \to \eta e\nu) = (2.28 \pm 0.14 \pm 0.19)\%$, and $\mathcal{B}(D_s \to \eta' e\nu) = (0.68 \pm 0.15 \pm 0.06)\%$ for the largest modes, where the first uncertainties are statistical and the second are systematic. We also obtain $\mathcal{B}(D_s \to K^0 e\nu) = (0.39 \pm 0.08 \pm 0.03)\%$, $\mathcal{B}(D_s \to K^* e\nu) = (0.18 \pm 0.04 \pm 0.01)\%$, and $\mathcal{B}(D_s \to f_0 e\nu, f_0 \to \pi\pi) = (0.13 \pm 0.03 \pm 0.01)\%$ for f_0 masses within 60 MeV of 980 MeV. We use our results to determine the $\eta - \eta'$ and f_0 mixing angles with $s\bar{s}$, and we combine our results with lattice calculations to estimate $|V_{cs}|$. This measurement improves upon the D_s semileptonic branching ratio precision and provides a new approach for future work that eliminates the D_s^* daughter photon reconstruction.

PACS numbers: 13.20.Fc, 12.38.Qk, 14.40.Lb

I. INTRODUCTION

D_s semileptonic decays have applications in both QCD tests and light meson spectroscopy. Most notably, exclusive D_s decays to the dominant modes ($\phi e\nu$, $\eta e\nu$, $\eta' e\nu$) involve no light valence quarks and thus provide an ideal opportunity for comparisons to lattice QCD results [1, 2]. Additionally, since the D_s primarily couples to the final state hadron's $s\bar{s}$ component, D_s decay rates can probe the quark content of $\eta - \eta'$ [3, 4] and of the scalar f_0 [5–7] (including possible glue components [8, 9]).

Further, inclusive semileptonic width measurements of strange and non-strange D mesons have revealed an interesting gap. The widths for $D^\pm, D^0$, and D_s decays should be equal in the Operator Product Expansion (OPE), up to SU(3) symmetry breaking and nonfactorizable components [10] (although phase space considerations may not be trivial [11]). While the $D^\pm$ and D^0 inclusive widths are consistent with each other, the D_s inclusive semileptonic width [12] falls some 16% lower, outside the range of experimental error. As the few lowest lying resonances dominate D^0 and possibly D^+ semileptonics [13–15], a higher precision measurement of the analogous modes in D_s semileptonics could shed light on this difference.

Although D_s exclusive semileptonic rates have been previously studied [16–18], the earlier measurements used relative branching fractions and focused on only $D_s \to \phi e\nu$ or $D_s \to \phi\mu\nu$. These measurements are complicated by possible interference between the reference mode, $D_s \to \phi\pi$, and other $D_s \to KK\pi$ modes. BaBar [19] has more recently obtained $\mathcal{B}(D_s \to \phi e\nu) = (2.61 \pm 0.03 \pm 0.17)\%$ in a relative measurement using a 10 MeV mass requirement for $\phi \to KK$ and taking $D_s \to KK\pi$ as their reference mode. In addition to its inclusive D_s semileptonic measurement [12], CLEO-c has determined absolute branching fractions for six D_s exclusive semileptonic modes in a partial (310 pb^{-1}) data sample [20] and performed another analysis for $D_s \to \phi e\nu$ and $D_s \to f_0 e\nu$ over a larger sample (600 pb^{-1}) [21]. Our analysis improves upon these results by using a novel technique that increases the efficiency for all semileptonic modes and eliminates a limiting systematic in prior measurments.

We use a data sample with an integrated e^+e^- luminosity of 586 pb^{-1} at a 4170 MeV center-of-mass energy, collected in the CLEO-c detector [22, 23]. The detector provided both charged and neutral particle identification. Charged particles followed a helical path through the detector's drift chamber under the uniform 1.0 Tesla magnetic field, allowing particle tracking, momentum determination, and mass identification from the specific ionization (dE/dx). A Ring-Imaging Cherenkov detector (RICH) improved charged particle identification for higher momentum tracks, where dE/dx does not give good separation. The RICH measured the light cone given off by particles passing through a LiF radiator, with an opening angle determined by the particle velocity. CLEO's CsI electromagnetic calorimeter detected photons, measuring their energy and direction. The calorimeter also contributed to identifying electrons through E/p, the energy deposited by a charged particle in the calorimeter relative to its momentum. Drift chamber tracks had a momentum resolution of 0.35% at 1 GeV, while calorimeter energy measurements had a resolution of about 4% at an energy of 100 MeV and about 2.2% at an energy of 1 GeV. [24]

* justinh@physics.umn.edu
† hennessy@physics.umn.edu

II. $D_s^* D_s$ EVENT IDENTIFICATION

Most D_s production in electron-positron collisions at a 4170 MeV center-of-mass energy comes in the form of $D_s^* D_s$ events with a cross section of 0.92 nb, while $D_s D_s$ events make up another 0.03 nb [25]. By contrast, the cross section to other charm events totals around 9 nb, with another 12 nb for *uds* continuum. To cleanly separate candidate D_s events from other charm and continuum, we completely reconstruct, or *tag*, one of the D_s mesons in the event. We use 13 different D_s decay modes in our tag reconstruction, listed in Table I.

TABLE I. Tag modes and counts. We list tag modes using their charges in D_s^+ decays for clarity, although the number of tags column contains the sum of results from both D_s^+ and D_s^-. The listed error is statistical.

D_s^+ mode	Number of tags
$K_S K^+$	6,227 ± 101
$K^+ K^- \pi^+$	27,374 ± 248
$K_S K^+ \pi^0$	2,247 ± 210
$K_S K_S \pi^+$	1,126 ± 77
$K^+ K^- \pi^+ \pi^0$	7,356 ± 377
$K_S K^+ \pi^+ \pi^-$	1,859 ± 121
$K_S K^- \pi^+ \pi^+$	3,377 ± 100
$\pi^+ \pi^+ \pi^-$	6,606 ± 338
$\pi^+ \eta$	3,810 ± 191
$\pi^+ \pi^0 \eta$	9,477 ± 529
$\pi^+ \eta', \eta' \to \pi^+ \pi^- \eta$	2,387 ± 66
$\pi^+ \pi^0 \eta', \eta' \to \pi^+ \pi^- \eta$	1,091 ± 119
$\pi^+ \eta', \eta' \to \rho^0 \gamma$	4,272 ± 193
Sum	77,208 ± 880

The D_s^* decays to $D_s \gamma$ about 95% of the time. The most common state produced in D_s events then contains a D_s^+, a D_s^-, and a photon. The standard approach would involve a tag consisting of one D_s and the D_s^* daughter photon, leaving just the other D_s. However, the D_s^* daughter photon reconstruction causes both an efficiency loss (about 1/3 are lost) and a high fake rate (about 50% of the true total), with nontrivial systematic effects given the accuracy of calorimeter simulations for low energy deposition. We consequently do not reconstruct the D_s^* daughter photon. This significantly improves our signal statistics and reduces the problematic photon fakes, albeit at the expense of a clean neutrino missing mass on the semileptonic side. Given the low backgrounds from our D_s and electron selections, however, we see a net improvement in our error by dropping the D_s^* daughter photon, using only the reconstructed D_s as our tag, and constructing an alternate method for signal determination (described in Sec. III).

Each tag mode's daughter particles have various track and shower quality requirements to ensure proper D_s reconstruction. Each fitted track must come within 5 mm of the interaction point in the radial direction and within 5 cm in the beam direction. Each track must also have at least 50% of the expected drift chamber wire hits and fall within the drift chamber's fiducial volume ($|\cos\theta| < 0.93$, with θ measured from the beamline). Candidate pions are required to have momenta above 50 MeV or 100 MeV (depending on the mode's background) to avoid double counting by swapping soft pions with the other side D_s. Candidate kaons must have a momentum above 125 MeV. Each track must have a dE/dx consistent with its mass hypothesis to within three standard deviations (3σ), and we add a combined RICH and dE/dx requirement for tracks in the RICH fiducial region ($|\cos\theta| < 0.8$) when dE/dx does not give good separation (momenta above 700 MeV). Our photon candidates (including π^0 and η daughters) must have shower energies above 30 MeV, and no tracks may lead to that shower.

Intermediate resonances receive additional selections. Our $\pi^0 \to \gamma\gamma$ and $\eta \to \gamma\gamma$ candidates must have a pull mass (standard deviation from nominal mass) within 3σ, and the η may not have both daughter showers detected in the calorimeter's endcap region ($0.85 < |\cos\theta| < 0.93$). Candidate K_S must have a mass within 6.3 MeV (1.6σ) of their nominal value. Our $\eta' \to \pi\pi\eta$ decays must involve a reconstructed η' mass within 10 MeV of its nominal value. The $\eta' \to \rho^0\gamma$ mode has the wider mass requirement that the η' mass falls between 920 MeV and 995 MeV, with a ρ mass between 0.5 GeV and 1.0 GeV. We also require individual tag mode selections to reject particular backgrounds. Specifically, no subset of particles may form a D^0 or $D^\pm$ to avoid D^* events (e.g. in $KK\pi\pi^0$, the $KK\pi$ mass can not fall between 1860 MeV and 1880 MeV); two pions may not form a K_S invariant mass except when explicitly desired; and in the $\pi\pi\pi$ mode, treating a reconstructed pion as a kaon can not form a D^0 mass with one of the other pions.

As a final restriction on our D_s tag candidates, we ensure that they have a momentum consistent with a $D_s^* D_s$ event through their recoil mass. The D_s recoil mass is defined by

$$M_{\rm recoil} \equiv |p_{\rm cm} - p_{D_s}| = \sqrt{\left(E_{\rm cm} - \sqrt{|\mathbf{p_{D_s}}|^2 + M_{D_s}^2}\right)^2 - |\mathbf{p}_{\rm cm} - \mathbf{p_{D_s}}|^2}, \quad (1)$$

where $p_{\rm cm}, E_{\rm cm}$, and $\mathbf{p}_{\rm cm}$ correspond to the center-of-mass four vector, energy, and momentum, respectively;

M_{D_s} is the nominal D_s mass; and $\mathbf{p_{D_s}}$ denotes the reconstructed D_s momentum. The recoil mass corresponds to the D_s^* mass for prompt D_s in $D_s^* D_s$, and it is fairly uncorrelated with the reconstructed invariant mass. We require a minimum recoil mass of 2.051 GeV for $K_S K$, $KK\pi$, $\pi\eta$, and $\pi\eta', \eta' \to \pi\pi\eta$; a minimum recoil mass of 2.101 GeV for $\pi\pi\pi$; and a minimum recoil mass of 2.099 GeV for all other tag modes. We only keep the best D_s candidate for each charge, as determined by the recoil mass closest to the D_s^* mass (2.112 GeV). This procedure successfully reconstructs around 7.2% of all prompt D_s decays and around 5.7% of all secondary D_s decays (those where the D_s came from a D_s^*, broadening their momentum distribution).

To obtain our total D_s tag counts, we fit the D_s invariant mass spectrum for each tag mode, as shown in Figure 1. We model our signal shape with either the sum of two Gaussians (a double Gaussian) or a Gaussian added to another with a power law tail (a Gaussian+Crystal Ball [26]). The tag modes $K_S K$, $KK\pi$, $K_S K_S \pi$, $K_S K^+ \pi\pi$, $K_S K^- \pi\pi$, and $\pi\eta', \eta' \to \pi\pi\eta$ each receive the double Gaussian signal shape, while the other modes receive the Gaussian+Crystal Ball signal shape. We use a quadratic background for $KK\pi\pi^0$, $\pi\pi\pi$, $\pi\pi^0\eta$, and $\pi\eta', \eta' \to \rho^0\gamma$, with a linear background for the other tag modes. Table I gives the tagged D_s counts resulting from our fits.

III. SEMILEPTONIC RECONSTRUCTION

Each semileptonic reconstruction involves an electron (positron) identification. We use three parameters in a weighted combination to identify a track as an electron. The most useful separation comes from the energy deposited in the calorimeter relative to the particle's momentum, E/p. We also include the particle's specific ionization in the drift chamber (dE/dx) and RICH information. Our electron efficiency varies by semileptonic mode but generally falls between 60%–70%, with most of the efficiency loss coming from a requirement that the electrons have momenta above 200 MeV (above the pion and electron dE/dx crossing). Only 0.1% of kaons in the appropriate momentum range successfully fake an electron, while pions fake less than 0.01% of the time.

We also require that no semileptonic event have tracks from the interaction point other than those accounted for in the tagged D_s, the electron, and the semileptonic-side hadron. We considered a similar constraint on extra energy in the calorimeter but did not find it useful given the spurious showers that accompany hadronic interactions.

Five of our six exclusive semileptonic measurements use a similar technique. $D_s \to \phi e\nu$, $D_s \to \eta' e\nu$, $D_s \to K^0 e\nu$, $D_s \to K^* e\nu$, and $D_s \to f_0 e\nu$ all involve finding the D_s tag, the semileptonic-side electron, and the semileptonic-side hadron, then fitting the tagged D_s invariant mass spectrum for the total number of semileptonic events. In these modes, low backgrounds allow us to determine the event counts without directly incorporating the semileptonic-side hadron's kinematic information into the fit. $D_s \to \eta e\nu$ does see significant background from photon fakes, so we instead perform a two-dimensional fit to the tagged D_s invariant mass and the η pull mass.

A. $D_s \to (\phi, \eta', K^0, K^*, f_0) e\nu$

We reconstruct our semileptonic-side hadrons through the modes $\phi \to KK$; $\eta' \to \pi\pi\eta, \eta \to \gamma\gamma$; $K^0 \to K_S \to \pi\pi$; $K^* \to K\pi$; and $f_0 \to \pi\pi$. We require the same daughter particle selections as for D_s tags, with a few exceptions. Our $\phi \to KK$ decays produce soft kaons that can decay in flight. Consequently, we remove the requirement that the drift chamber has 50% or more of the expected hits. We also do not use the RICH information for kaons from a ϕ. The $K^* \to K\pi$ decay has a similar (but less severe) soft kaon problem, so we relax its kaon hit requirement to 30%. We apply a flight significance selection in $K_S \to \pi\pi$ decays to ensure that the daughter pions did not come from the interaction point ($\pi\pi$ vertex more than 4σ from the interaction point). We also add a maximum flight distance of 20 cm to avoid fake K_S created near the calorimeter. Given the low backgrounds, we implement loose mass selections on our resonances: the reconstructed ϕ mass must be within 15 MeV of the nominal mass on the low side and 30 MeV on the high side (-15 MeV $< M_\phi^{\rm recon} - M_\phi^{\rm nom} < 30$ MeV), avoiding sensitivity to resonance effects near KK threshold while retaining the high-side mass tail; the reconstructed η' mass must fall within 10 MeV of its nominal value; K_S follows the 6.3 MeV mass cut listed with our tags; the K^* mass must be within 106 MeV of its nominal value; and the f_0 mass must be within 60 MeV of 980 MeV.

We see some background in our exclusive semileptonic modes from other D_s semileptonic decays (e.g. $D_s \to f_0 e\nu, f_0 \to KK$ background in $D_s \to \phi e\nu$; $D_s \to \phi e\nu, \phi \to K_S K_L$ background in $D_s \to K^0 e\nu$). For $\phi e\nu$, we use our measured $D_s \to f_0 e\nu$ branching fraction and Monte Carlo simulations with a Flatté model [27, 28] to correct our observed branching fraction. In $K^* e\nu$ and $K^0 e\nu$, we cut on the "missing mass," which here corresponds to the invariant mass of the neutrino and the D_s^* photon. This selection (mass squared below 0.4 GeV^2 for $K^0 e\nu$ and below 0.45 GeV^2 for $K^* e\nu$) distinguishes signal from background events with a missing K_L. Finally, we ensure that we do not have $\phi e\nu$, $\phi \to KK$ faking $K^* e\nu$, $K^* \to K\pi$ by treating the K^* pion as a kaon and vetoing candidates with an invariant KK mass less than 1.06 GeV. We apply an explicit correction for remaining background from other D_s semileptonic modes by using the background mode's measured branching ratio and the efficiency with which it fakes the target mode's selections. We additionally correct for the small number of events (0.10–1.25, depending on semileptonic mode) with a true D_s but a false hadron or non-semileptonic

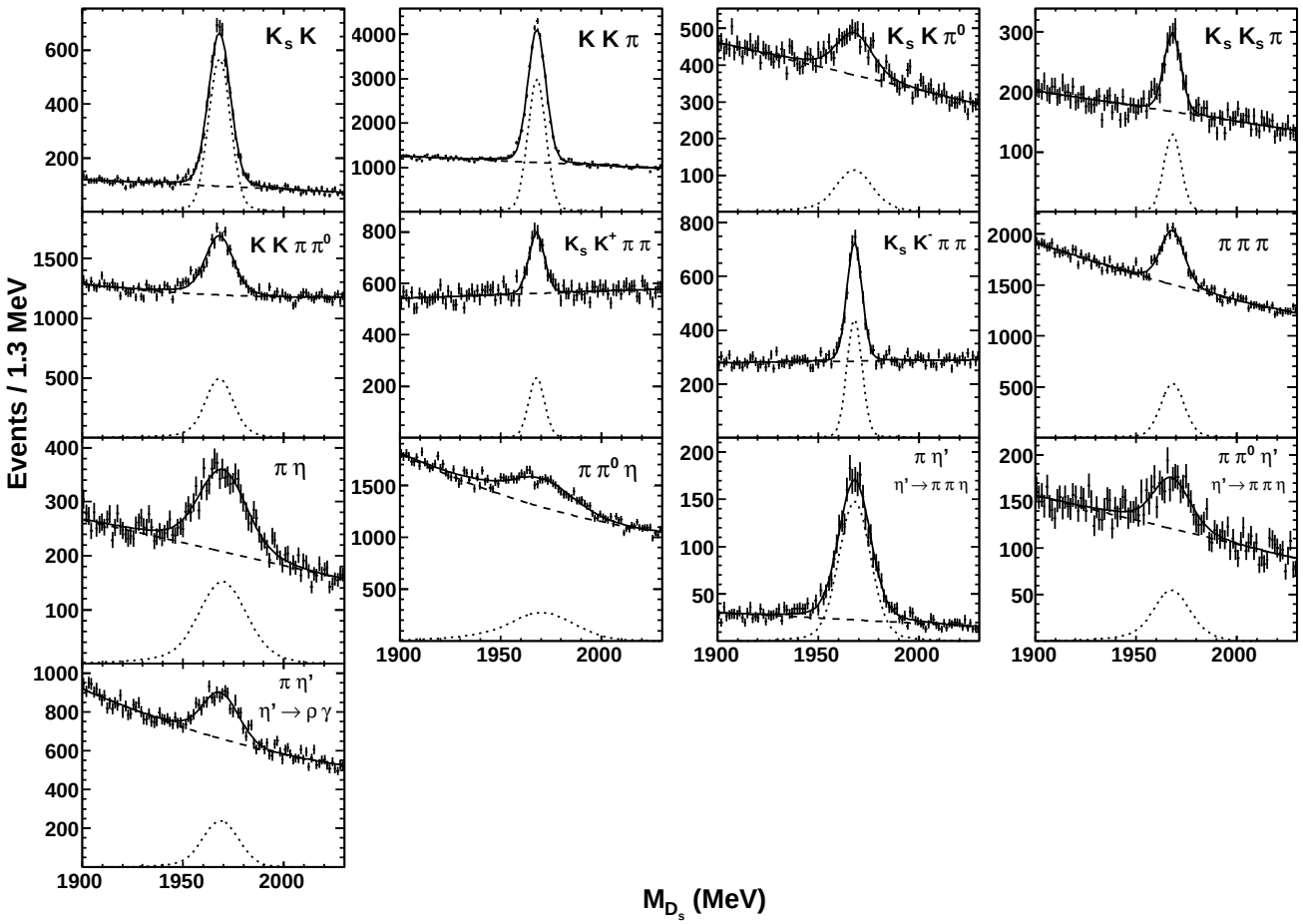

FIG. 1. Invariant D_s mass for each of our 13 tag modes. Points with error bars represent the data, the solid line represents our total fit, and the dotted and dashed lines give our signal and background fit components, respectively.

electron using Monte Carlo predictions, cross-checked by data comparisons in the hadronic mass sideband and alternate reconstructions for the electron.

After finding an event with a valid D_s tag, electron, and semileptonic-side hadron, we fit the tag's invariant mass. We take the signal shape for each D_s tag mode from the results of that mode's tagging fit. Each mode gets a linear or constant background based on our Monte Carlo prediction for combinatoric background. We then perform an unbinned, log likelihood fit on the data that is linked across the 13 tag modes by a common branching ratio constraint. Figure 2 shows the results of our fits, summed over all 13 tag modes.

B. $D_s \to \eta e \nu$

We reconstruct $D_s \to \eta e \nu$ through $\eta \to \gamma\gamma$. We use the same selections as for η in our D_s tags except for the pull mass requirement, which we relax to 5σ to give sufficient sideband regions in our fits. After reconstructing the η, we also implement a missing mass squared maximum of 0.5 GeV^2 to avoid backgrounds from other semileptonic modes that decay to η (like $D_s \to \eta' e\nu$, $\eta' \to \pi^0\pi^0\eta$).

We see several "volunteer" events in our $D_s \to \eta e\nu$ reconstruction, where a true event gets reconstructed incorrectly. This happens when the D_s^* daughter photon or a photon fake combines with a true η daughter photon to make a false η combination, either in addition to the true combination or as the only combination when the true η was missed. While the D_s^* daughter photon volunteer rate can be determined from kinematics, the volunteer rate from fake photon combinations depends upon detector effects that are not well understood. We explicitly estimate the rate of these volunteer events by reconstructing $D^0 \to K^*\eta$ in the much larger 3770 MeV CLEO-c sample and incorporate the η volunteer rate from that data's result into our fits.

We then perform a two-dimensional fit to the reconstructed D_s tag mass and the η pull mass. As before, we use the results of our D_s tagging fits to fix the D_s invariant mass shape. We take our signal η shape from the

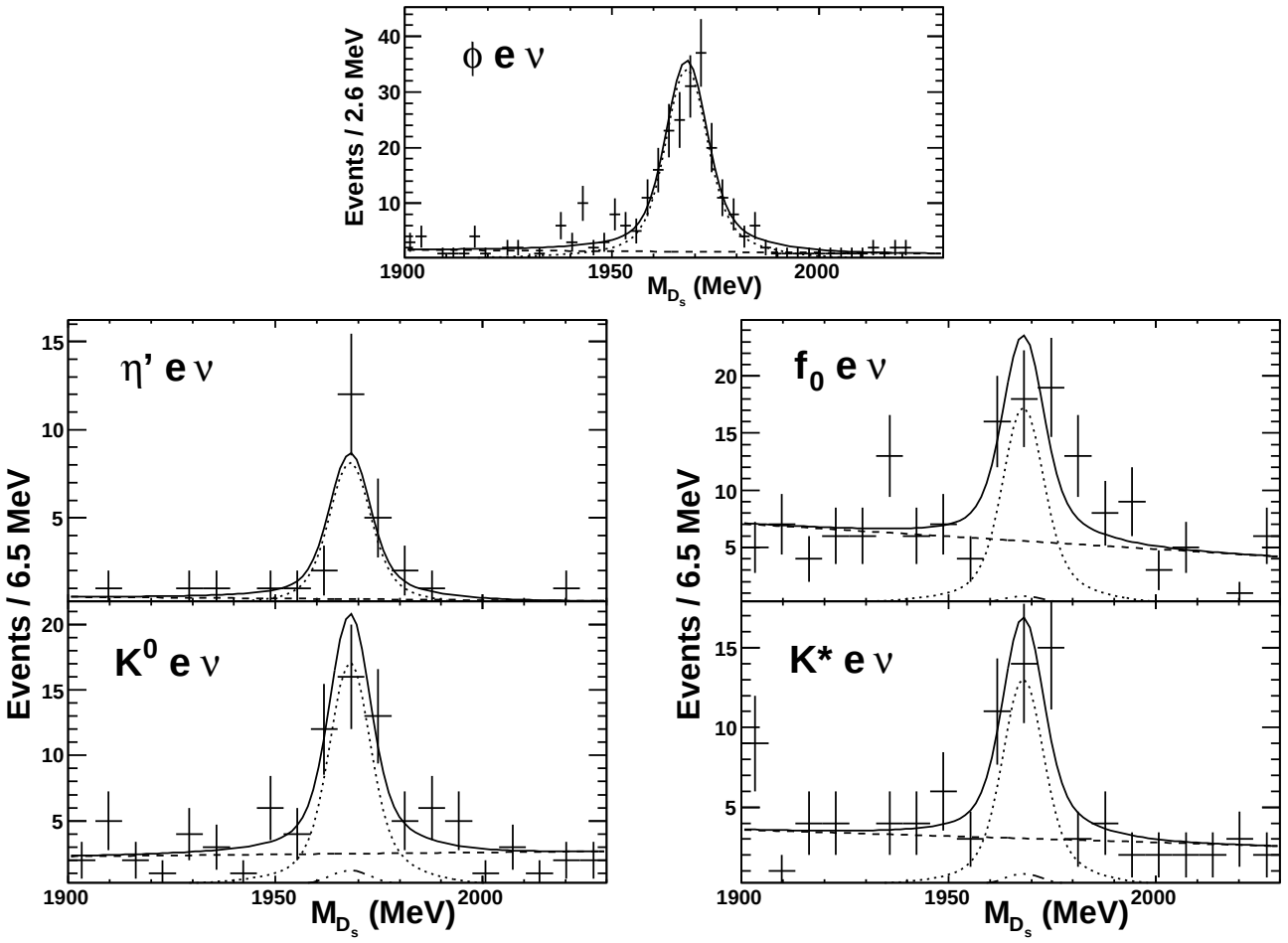

FIG. 2. Tagged D_s invariant mass summed over all modes after semileptonic selections for $\phi e\nu$, $\eta' e\nu$, $f_0 e\nu$, $K_S e\nu$, and $K^* e\nu$. Crosses represent data, while the solid line gives our total fit. The dotted line shows the signal part of our fit, the dashed line gives combinatoric background, and the small, peaking component represented by the dashed-dot line gives our background from other D_s semileptonic modes.

Monte Carlo. Both the tag and the η pull mass fits receive linear background functions. We generate our two-dimensional fit function by multiplying the signal and background tag functions by the signal and background η functions, taking separate normalizations for each tag's background modes and using a common branching ratio for the signal shapes across each tag mode. We constrain our true D_s, false η using our $D^0 \to K^*\eta$ study's volunteer rate, adjusted for the number of kaons and pions in the D_s tag mode.

Figure 3 shows the D_s mass and η pull mass projections of our two-dimensional fits.

C. Systematic Uncertainties

Our dominant systematic errors (those with a relative error above 1%) come from particle reconstruction, particularly from the soft kaons frequently produced in $D_s \to \phi e\nu$ and $D_s \to K^* e\nu$ decays (around 2%); the D_s tag fits' signal shapes (2%); the effect of our Monte Carlo's form factor model on predicted efficiencies (1%–3%); the choice of a best candidate for the recoil mass (0%–3%); the mass resolution on our η', K^*, and f_0 selections (3%); the correction from other D_s semileptonic modes (0%–2%); soft K_S reconstruction in $D_s \to K_S e\nu$ (7%); and η reconstruction via two photons in $D_s \to \eta e\nu$ and $D_s \to \eta' e\nu$ (8%).

We use $D^\pm \to K^\mp\pi^\pm\pi^\pm$ decays at 3770 MeV to estimate the systematic error for charged kaon reconstruction, including particle identification. We reconstruct a $D^\pm$ tag, then find an additional $\pi^\mp\pi^\mp$. We fit the recoil mass spectrum for events when we successfully reconstruct a kaon using our selections and again for events when we did not reconstruct a kaon, giving us our kaon efficiency. We perform this procedure for kaons of different momenta (determined by the recoil momentum) and correct our Monte Carlo efficiency in each momentum

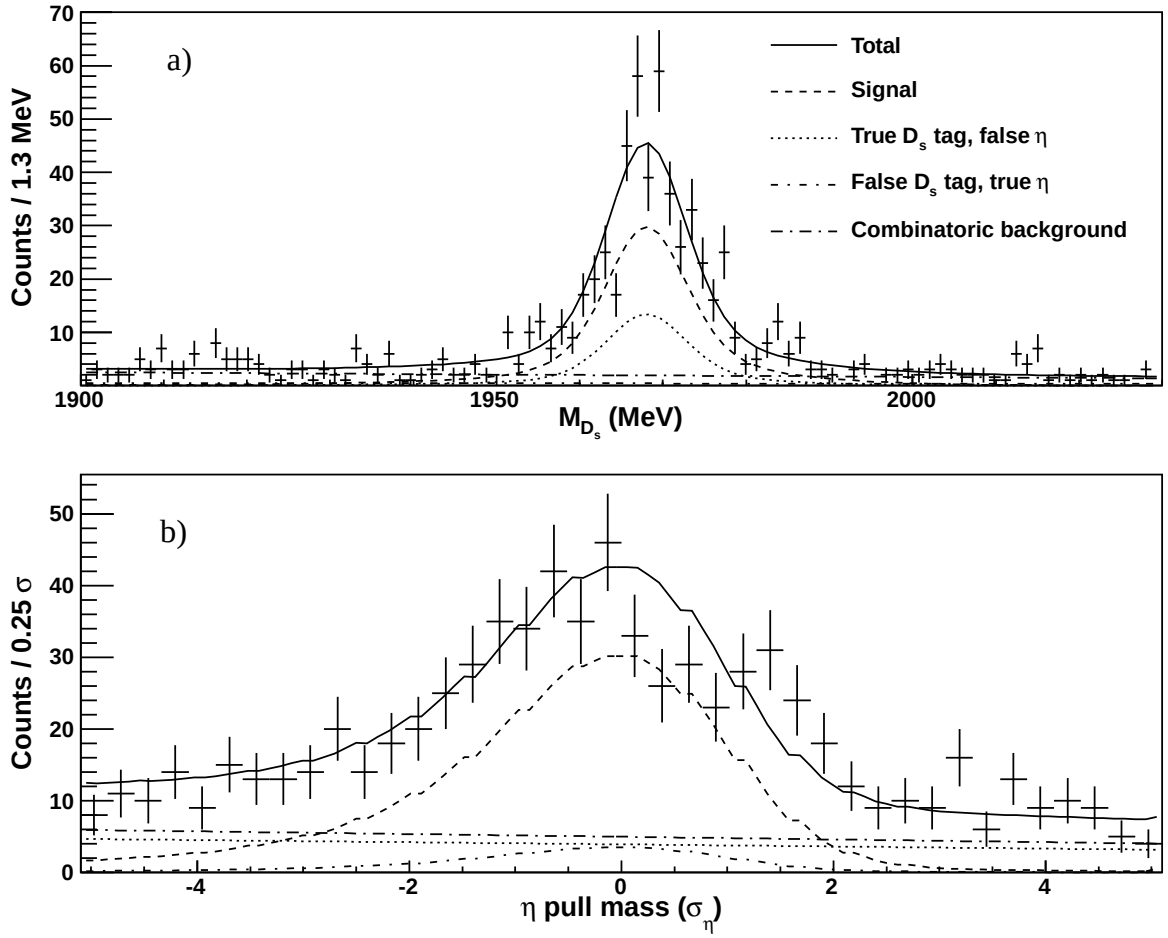

FIG. 3. Our $D_s \to \eta e\nu$ reconstruction's two dimensional fit projections for (a) invariant D_s mass and (b) η pull mass. Crosses represent data, while the lines show our total fit result and its four fit components.

range accordingly.

We apply a similar approach for our K_S reconstruction systematic, although we need to use two modes to cover the full K_S momentum range: $D_s \to K_S K^{\mp}\pi^{\pm}\pi^{\pm}$ (K^*K^*) for lower momentum K_S and $D_s \to K_S K$ for higher momentum K_S. We again reconstruct all particles but the K_S (including the D_s^* daughter photon), use the recoil momentum to determine the underlying K_s momentum region, and fit the recoil mass for found and not found K_S to determine the Monte Carlo efficiency in each K_S momentum range.

Our η reconstruction systematic takes advantage of the relatively high $D_s \to \pi\pi^0\eta$ rate, where we reconstruct the D_s tag, the D_s^* daughter photon, and a $\pi\pi^0$ combination. To avoid complications from the D_s^* photon resolution, we perform a two-dimensional fit to the $D_s + \gamma$ recoil mass and the $D_s + \gamma + \pi\pi^0$ recoil mass for our candidate events. We then do another two-dimensional fit to the $D_s + \gamma + \pi\pi^0$ recoil mass and η pull mass for our succesfully reconstructed η candidates. The ratio of these fits gives us our efficiency for η reconstruction and the associated systematic error.

We determine the uncertainty on our D_s tag fits' signal shapes by reconstructing analogous modes in the high-yield $D^{\pm}$ system and adjusting the D_s fit functions' fixed parameters (relative normalization and relative width for the double Gaussian/Gaussian+Crystal Ball) to match the measured $D^{\pm}$ mass resolutions in data. We estimate the systematic error on our D_s tag fits' background shapes by using the Monte Carlo predicted backgrounds in place of our linear or quadratic backgrounds.

To estimate the effects of an improper Monte Carlo mass resolution on our η', K^*, and f_0 intermediate resonances, we use the reconstructed resolution from the clean modes $D_s \to \pi\eta'$, $D_s \to K^*K$, and $D_s \to f_0\pi$, respectively. We generated Monte Carlo using both the ISGW2 form factor model [29] and a simple pole model, then took the efficiency difference between the two as our standard deviation for the semileptonic efficiency's systematic due to uncertain form factors.

IV. RESULTS

Table II gives the branching ratio results for each of our six semileptonic modes, along with their efficiencies and number of signal events. These results improve the existing precision by about 20% for the largest modes, $\phi e\nu$ and $\eta e\nu$, and by up to 40% for the smaller branching fraction modes (other than f_0, which has special considerations discussed below). The sum of our exclusive modes has a branching fraction of $(5.80 \pm 0.27 \pm 0.30)\%$, which falls below the inclusive rate of $(6.52 \pm 0.39 \pm 0.15)\%$ by 1.2σ, possibly leaving a small role for semileptonic decays with multiple hadrons.

Table III shows how this analysis's results compare to prior results. Our $D_s \to f_0 e\nu$, $f_0 \to \pi\pi$ results give the branching fraction for only $f_0 \to \pi\pi$ that fall within a ± 60 MeV mass window to avoid complications from the uncertain f_0 width and the onset of nonlinear backgrounds at low f_0 masses. The previous analysis fit the $\pi\pi$ mass spectrum over a wide range for their f_0 result. Both results are consistent if we apply a ± 60 MeV mass requirement to their data as well.

V. DISCUSSION

Various theoretical predictions have been made for relative or absolute D_s semileptonic decay rates [1, 4–7, 11, 29–34]. Some predictions combine with our measured results to determine meson mixing angles. For instance, if we take η and η' to be purely $q\bar{q}$ states, the D_s semileptonic decays to η and η' can extract the $\eta - \eta'$ mixing angle. For the mixing angle defined by

$$\begin{aligned} |\eta'\rangle &= \sin\phi\,|n\bar{n}\rangle + \cos\phi\,|s\bar{s}\rangle \\ |\eta\rangle &= \cos\phi\,|n\bar{n}\rangle - \sin\phi\,|s\bar{s}\rangle \end{aligned} \tag{2}$$

with $|n\bar{n}\rangle = \frac{1}{\sqrt{2}}\left|u\bar{u} + d\bar{d}\right\rangle$, the ratio of semileptonic widths gives [3]

$$\frac{\Gamma(D_s \to \eta' e\nu)}{\Gamma(D_s \to \eta e\nu)} = R_D \cot^2\phi, \tag{3}$$

where R_D contains the relative phase space and the ratio of integrated form factors. Anisovich, et al. [8] have used a monopole quark transition form factor to estimate $R_D = 0.23$, which combines with our result to give an $\eta - \eta'$ mixing angle of $\phi = 41^\circ \pm 4^\circ$. If the constituent quark transition form factor ratio is instead taken to be unity, $R_D = 0.28$ and we get $\phi = 44^\circ \pm 4^\circ$.

We can compare these results to the $SU(3)$ mixing angle given by

$$\begin{aligned} |\eta'\rangle &= \sin\theta\,|\eta_0\rangle + \cos\theta\,|\eta_8\rangle \\ |\eta\rangle &= \cos\theta\,|\eta_0\rangle - \sin\theta\,|\eta_8\rangle\,, \end{aligned} \tag{4}$$

where the singlet and octet states follow $|\eta_0\rangle = \frac{1}{\sqrt{3}}\left|u\bar{u} + d\bar{d} + s\bar{s}\right\rangle$ and $|\eta_8\rangle = \frac{1}{\sqrt{6}}\left|u\bar{u} + d\bar{d} - 2s\bar{s}\right\rangle$. The bases relate to each other through $\theta = \phi - \arctan\sqrt{2}$, with $\theta = 0$ corresponding to $SU(3)$ symmetry. In the $SU(3)$ basis, our results become $\theta = -13^\circ \pm 4^\circ$ with the monopole form factor and $\theta = -11^\circ \pm 4^\circ$ for the flat form factor.

Alternately, the assumption of an η' state consisting of only $q\bar{q}$ can be loosened by allowing for a glue component. In this case, we can use D^+ semileptonic decays to cancel the glue component through the ratio [3]

$$\frac{\Gamma(D_s \to \eta' e\nu)/\Gamma(D_s \to \eta e\nu)}{\Gamma(D^+ \to \eta' e\nu)/\Gamma(D^+ \to \eta e\nu)} = \cot^4\phi. \tag{5}$$

Here, the phase space and form factor ratio R_D is assumed to be the same for D^+ and D_s decays. Combining our D_s results with the D^+ data [35] gives $\phi = 42^\circ \pm 2^\circ \pm 2^\circ$ ($\theta = -13^\circ \pm 2^\circ \pm 2^\circ$), where the first error comes from the D^+ measurement and the second comes from our measurement.

The f_0 mixing angle, defined by

$$|f_0\rangle = \sin\theta\,|n\bar{n}\rangle + \cos\theta\,|s\bar{s}\rangle\,, \tag{6}$$

may also be extracted by comparisons to theoretical calculations. Several such estimates of the f_0 decay rate exist [5–7], which collectively set the branching fraction at $\mathcal{B}(D_s \to f_0 e\nu) = (0.41\text{–}0.55)\% \times \cos^2\theta$. We use a Flatté model with a Γ_{f_0} range from 50 MeV–100 MeV, an M_{f_0} range from 970 MeV–990 MeV, and $\Gamma(f_0 \to K^+K^-)/\Gamma(f_0 \to \pi^+\pi^-)$ values taken from experiment [36, 37] to estimate the fraction of $f_0 \to \pi^+\pi^-$ in our ± 60 MeV window. These combine with our $D_s \to f_0 e\nu$ measurement to yield an $s\bar{s}$ mixing angle of $\cos^2\theta = 0.94 \pm 0.26 \pm 0.07 \pm 0.19$, where the first error comes from the range of predictions, the second error comes from the uncertain f_0 mass and width, and the third error comes from our measurement. Ignoring the nonphysical range and treating the errors as independent gives a mixing angle of $\theta = 20^\circ{}^{+32^\circ}_{-20^\circ}$.

As a simple example of using our $D_s \to \phi e\nu$ measurement in conjunction with a lattice calculation, we determine a $|V_{cs}|$ value [1]. We use [38]

$$\frac{\mathcal{B}(D_s \to \phi e\nu)}{|V_{cs}|^2} = (2.52 \pm 0.22 \pm 0.15)\%, \tag{7}$$

where the first error comes from the $D_s \to \phi e\nu$ lattice simulation, and the second error comes from complications due to the strong $\phi \to KK$ decay (not a "gold-plated" decay). This yields $|V_{cs}| = 0.921 \pm 0.041 \pm 0.049$, with our measurement uncertainty generating the first error and the combination of both lattice uncertainties giving the second error. The $|V_{cs}|$ result falls within one standard deviation of the best current value (0.986 ± 0.016) [15].

TABLE II. Number of signal events, efficiencies (including all hadron branching fractions, like $\phi \to K^+K^-$), and final branching fractions for each semileptonic mode. We list our statistical error first, followed by our systematic error (combining both for the systematics-dominated efficiency error). Each mode uses $77,208 \pm 880 \pm 1,675$ D_s tags. We have a soft correlation between the tags' systematic error and the systematic error on the number of signal events due to using a common D_s shape. We also have a moderate correlation in the systematic between semileptonic modes that is reflected in our sum's systematic error.

Signal mode	$N_{\rm sig}$	$\varepsilon_{s\ell}$	$\mathcal{B}(\%)$
$D_s \to \phi e\nu$	206.7 ± 16.4 ± 2.3	(12.5 ± 0.5)%	2.14 ± 0.17 ± 0.08
$D_s \to \eta e\nu$	358.2 ± 21.6 ± 6.8	(20.4 ± 1.7)%	2.28 ± 0.14 ± 0.19
$D_s \to \eta' e\nu$	20.1 ± 4.4 ± 0.3	(3.8 ± 0.4)%	0.68 ± 0.15 ± 0.06
$D_s \to f_0 e\nu, f_0 \to \pi\pi$	41.9 ± 7.8 ± 0.6	(21.2 ± 1.0)%	0.13 ± 0.03 ± 0.01
$D_s \to K^0 e\nu$	41.5 ± 8.3 ± 0.5	(13.7 ± 1.1)%	0.39 ± 0.08 ± 0.03
$D_s \to K^* e\nu$	31.6 ± 7.5 ± 0.4	(23.0 ± 1.4)%	0.18 ± 0.04 ± 0.01
Sum			5.80 ± 0.27 ± 0.30

TABLE III. Most recent exclusive D_s semileptonic branching fraction measurements. Each of our modes is consistent with the previous CLEO-c measurements [20, 21], including statistical and systematic correlations (1.2 standard deviations for $D_s \to \phi e\nu$). However, we see an inconsistency with BaBar's result [19] in $D_s \to \phi e\nu$. Note that the $D_s \to f_0 e\nu$ rates involve different f_0 mass cuts; the CLEO-c branching fraction with a ±60 MeV mass cut matches our result to within one standard deviation.

Signal mode	BaBar (%)	CLEO-c (%)	This analysis (%)
$D_s \to \phi e\nu$	2.61 ± 0.03 ± 0.08 ± 0.15	2.36 ± 0.23 ± 0.13	2.14 ± 0.17 ± 0.08
$D_s \to \eta e\nu$	—	2.48 ± 0.29 ± 0.13	2.28 ± 0.14 ± 0.19
$D_s \to \eta' e\nu$	—	0.91 ± 0.33 ± 0.05	0.68 ± 0.15 ± 0.06
$D_s \to f_0 e\nu, f_0 \to \pi\pi$	Seen	0.20 ± 0.03 ± 0.01	0.13 ± 0.03 ± 0.01
$D_s \to K_S e\nu$	—	0.19 ± 0.05 ± 0.01	0.20 ± 0.04 ± 0.01
$D_s \to K^* e\nu$	—	0.18 ± 0.07 ± 0.01	0.18 ± 0.04 ± 0.01

VI. CONCLUSION

We have used CLEO-c's 4170 MeV data to measure semileptonic decays for the six exclusive modes $D_s \to (\phi, \eta, \eta', f_0, K^0, K^*)e\nu$. Our procedure uses additional data for four modes ($\eta e\nu$, $\eta' e\nu$, $K^0 e\nu$, and $K^* e\nu$) and involves a new technique in which the D_s^* daughter photon does not get reconstructed, significantly increasing the available statistics. We see $\mathcal{B}(D_s \to \phi e\nu) = (2.14 \pm 0.17 \pm 0.08)\%$; $\mathcal{B}(D_s \to \eta e\nu) = (2.28 \pm 0.14 \pm 0.19)\%$; $\mathcal{B}(D_s \to \eta' e\nu) = (0.68 \pm 0.15 \pm 0.06)\%$; $\mathcal{B}(D_s \to K^0 e\nu) = (0.39 \pm 0.08 \pm 0.03)\%$; $\mathcal{B}(D_s \to K^* e\nu) = (0.18 \pm 0.04 \pm 0.01)\%$; and $\mathcal{B}(D_s \to f_0 e\nu, f_0 \to \pi\pi) = (0.13 \pm 0.03 \pm 0.01)\%$ within 60 MeV of the f_0 mass. Our measurements show that these six exclusive modes nearly saturate the inclusive D_s width.

We also combined our results with theoretical predictions and other measurements to extract an $\eta - \eta'$ mixing angle of $\phi = 42^\circ \pm 2^\circ \pm 2^\circ$ and an f_0 mixing angle with $s\bar{s}$ of $\theta = 20^{\circ\,+32^\circ}_{\;-20^\circ}$.

ACKNOWLEDGMENTS

We would like to thank M.B. Voloshin for useful discussions on D meson semileptonics, particularly inclusive decays. We thank G.P. Lepage for sharing some of his lattice knowledge wtih us. This analysis uses CLEO-c data; as members of the retired CLEO collaboration, we appreciate the afforded opportunity to revive it one more time. We also gratefully acknowledge the CESR staff for their efforts to provide the good run conditions and luminosity needed for this and all other CLEO work over four decades.

[1] G. Donald, C. Davies, J. Koponen, and G. Lepage (HPQCD), Phys. Rev. **D90**, 074506 (2014), arXiv:1311.6669 [hep-lat].
[2] S. Collins, I. Kanamori, and J. Najjar, in *Proceedings, 6th International Workshop on Charm Physics (Charm 2013)*, edited by M. Gersabeck and C. Parkes (Manchester U., 2014), arXiv:1311.7393 [hep-lat].
[3] C. Di Donato, G. Ricciardi, and I. Bigi, Phys. Rev. **D85**, 013016 (2012), arXiv:1105.3557 [hep-ph].
[4] P. Colangelo and F. De Fazio, Phys. Lett. **B520**, 78 (2001), arXiv:hep-ph/0107137 [hep-ph].
[5] T. Aliev and M. Savci, Europhys. Lett. **90**, 61001 (2010),

arXiv:hep-ph/0701108 [hep-ph].
[6] I. Bediaga and M. Nielsen, Phys. Rev. **D68**, 036001 (2003), arXiv:hep-ph/0304193 [hep-ph].
[7] H.-W. Ke, X.-Q. Li, and Z.-T. Wei, Phys. Rev. **D80**, 074030 (2009), arXiv:0907.5465 [hep-ph].
[8] V. Anisovich, D. Bugg, D. Melikhov, and V. Nikonov, Phys. Lett. **B404**, 166 (1997), arXiv:hep-ph/9702383 [hep-ph].
[9] H. G. Dosch and S. Narison, Nucl. Phys. Proc. Suppl. **121**, 114 (2003), arXiv:hep-ph/0208271 [hep-ph].
[10] M. Voloshin, Phys. Lett. **B515**, 74 (2001), arXiv:hep-ph/0106040 [hep-ph].
[11] M. Gronau and J. L. Rosner, Phys. Rev. **D83**, 034025 (2011), arXiv:1012.5098 [hep-ph].
[12] D. Asner *et al.* (CLEO Collaboration), Phys. Rev. **D81**, 052007 (2010), arXiv:0912.4232 [hep-ex].
[13] G. Huang *et al.* (CLEO Collaboration), Phys. Rev. Lett. **95**, 181801 (2005), arXiv:hep-ex/0506053 [hep-ex].
[14] N. Adam *et al.* (CLEO Collaboration), Phys. Rev. Lett. **97**, 251801 (2006), arXiv:hep-ex/0604044 [hep-ex].
[15] J. Beringer *et al.* (Particle Data Group), Phys. Rev. **D86**, 010001 (2012).
[16] P. Frabetti *et al.* (E687 Collaboration), Phys. Lett. **B313**, 253 (1993).
[17] F. Butler *et al.* (CLEO Collaboration), Phys. Lett. **B324**, 255 (1994), arXiv:hep-ph/9403328 [hep-ph].
[18] J. Link *et al.* (Focus Collaboration), Phys. Lett. **B541**, 243 (2002), arXiv:hep-ex/0206056 [hep-ex].
[19] B. Aubert *et al.* (BaBar Collaboration), Phys. Rev. **D78**, 051101 (2008), arXiv:0807.1599 [hep-ex].
[20] J. Yelton *et al.* (CLEO Collaboration), Phys. Rev. **D80**, 052007 (2009), arXiv:0903.0601 [hep-ex].
[21] K. Ecklund *et al.* (CLEO Collaboration), Phys. Rev. **D80**, 052009 (2009), arXiv:0907.3201 [hep-ex].
[22] Y. Kubota *et al.* (CLEO Collaboration), Nucl. Instrum. Meth. **A320**, 66 (1992).
[23] D. Peterson, K. Berkelman, R. A. Briere, G. Chen, D. Cronin-Hennessy, *et al.*, Nucl. Instrum. Meth. **A478**, 142 (2002).
[24] R. A. Briere *et al.* (CLEO Collaboration), (2001).
[25] D. Cronin-Hennessy *et al.* (CLEO Collaboration), Phys. Rev. **D80**, 072001 (2009), arXiv:0801.3418 [hep-ex].
[26] T. Skwarnicki, Ph.D. thesis, Institute of Nuclear Physics, Krakow, 1986.
[27] S. M. Flatte, Phys. Lett. **B63**, 224 (1976).
[28] S. M. Flatte, M. Alston-Garnjost, A. Barbaro-Galtieri, J. Friedman, G. Lynch, *et al.*, Phys. Lett. **B38**, 232 (1972).
[29] D. Scora and N. Isgur, Phys. Rev. **D52**, 2783 (1995), arXiv:hep-ph/9503486 [hep-ph].
[30] D. Melikhov and B. Stech, Phys. Rev. **D62**, 014006 (2000), arXiv:hep-ph/0001113 [hep-ph].
[31] Z.-T. Wei, H.-W. Ke, and X.-F. Yang, Phys. Rev. **D80**, 015022 (2009), arXiv:0905.3069 [hep-ph].
[32] K. Azizi, R. Khosravi, and F. Falahati, J. Phys. **G38**, 095001 (2011), arXiv:1011.6046 [hep-ph].
[33] P. Colangelo, F. De Fazio, and W. Wang, Phys. Rev. **D81**, 074001 (2010), arXiv:1002.2880 [hep-ph].
[34] M. Y. Khlopov, Sov. J. Nucl. Phys. **28**, 583 (1978).
[35] J. Yelton *et al.* (CLEO Collaboration), Phys. Rev. **D84**, 032001 (2011), arXiv:1011.1195 [hep-ex].
[36] B. Aubert *et al.* (BaBar Collaboration), Phys. Rev. **D74**, 032003 (2006), arXiv:hep-ex/0605003 [hep-ex].
[37] M. Ablikim *et al.* (BES Collaboration), Phys. Rev. **D72**, 092002 (2005), arXiv:hep-ex/0508050 [hep-ex].
[38] G. Lepage and C. Davies, private communication.